

A CONTINUUM/KINETIC HYBRID APPROACH FOR MULTI-SCALE FLOW SIMULATION

Koji Morinishi*

*Kyoto Institute of Technology, Department of Mechanical and System Engineering
Matsugasaki, Sakyo-ku, Kyoto 606-8585, Japan
e-mail: morinisi@kit.ac.jp
web page: <http://www.cis.kit.ac.jp/~morinisi>

Key words: Hybrid approach, Multi-scale flow, Navier-Stoke equations, Boltzmann equation, Micro-scale flow

Abstract. *This paper describes a continuum/kinetic hybrid approach for simulating the continuum to free molecule, multi-scale flows. Domain decomposition strategy is adopted for coupling the continuum and kinetic approaches. Instead of the direct simulation Monte Carlo method, a deterministic solver based on a kinetic model Boltzmann equation is adopted for kinetic regions, while a Navier-Stokes solver adopted for continuum regions. Reliable solution can be obtained for both subsonic and supersonic flows with the hybrid solver at lower computational costs compared to the direct simulation Monte Carlo method. Numerical results obtained with the hybrid solver have been compared with those of the Navie-Stokes solver for slip flow regime and those of the direct simulation Monte Carlo method for rarefied flow regime. The comparison is fairly good.*

1 INTRODUCTION

Numerical flow simulation about micro devices is one of the recent new frontiers of computational fluid dynamics (CFD). It may provides essential understanding about the fluid behavior around micro-electro-mechanical systems (MEMS). Since the flows about the micro devices range from continuum to free molecule, numerical methods designed for simulating the multi-scale flows, from continuum to free molecule flows, are preferable.

In the past decade, several studies about continuum/kinetic hybrid approaches have been reported [1-7]. Most of them are hybrid approaches using the Navier-Stokes (NS) method and the direct simulation Monte Carlo (DSMC) method [8]. These NS/DSMC hybrid methods, however, have severe deficiency caused from inherent statistical scatter of the DSMC method. A large number of sample size in the DSMC method is generally required to obtain the macroscopic flow quantities at every coupling time step between the NS method and DSMC method. The hybrid method may becomes a poor simulation tool for low speed flows about micro devices, because huge sample size may be required

to reduce the statistical scatter of DSMC method to a level of the small changes of flow quantities in the low speed flows [9, 10].

In contrast to the DSMC method, a numerical Boltzmann solver based on a kinetic model Boltzmann equation [11, 12] is free from the statistical scatter. The numerical Boltzmann solver is definitely superior to the DSMC method for simulating the subsonic flows, although it is rather expensive for hypersonic flow simulation [13]. Moreover a Navier-Stokes/Boltzmann hybrid method, an universal tool for analyzing continuum to molecule multi-scale flows, may be easily constructed, since the same CFD methods can be adopted for the kinetic model Boltzmann equation as well as the Navier-Stokes equations.

In this study, a novel continuum/kinetic hybrid solver is proposed for simulating the continuum to free molecule, multi-scale flows, by coupling the Navier-Stokes solver and the kinetic model Boltzmann solver. The rest of the paper is organized as follows. The kinetic approach is described in Section 2 and the continuum approach in Section 3. Section 4 describes the continuum/kinetic hybrid approach. Validation of the kinetic model Boltzmann solver as well as the Navier-Stokes solver is demonstrated numerically in Section 5. The validation of the continuum/kinetic hybrid approach is carried out in Section 6. Finally, Section 7 describes some concluding remarks.

2 KINETIC APPROACH

The motion of gas molecules at any Knudsen number is governed by the well known Boltzmann equation. In the transition regime from continuum to free molecular flows, especially, it is naturally desirable to obtain the solution of the Boltzmann equation instead of the Navier-Stokes equation. Because of its complex collision integral term, however, the solution of the Boltzmann equation requires an exceedingly formidable task except for few simple problems. In this paper, instead of the full Boltzmann equation, we use a kinetic model equation [14], which correctly resembles the lower 13 moments (the density, three components of the velocity, six components of the stress tensor, and three components of the heat flux) of the Boltzmann equations.

2.1 Kinetic model equation

The kinetic model Boltzmann equation in nondimensional form without any external force may be written as follows:

$$\frac{\partial f}{\partial t} + \mathbf{c} \cdot \frac{\partial f}{\partial \mathbf{x}} = \nu(f_0 - f) \quad (1)$$

where f is the velocity distribution function which depends on the time t , the physical space \mathbf{x} , and the molecular velocity \mathbf{c} . The distribution function f_0 of the BGK model [15], which is the most fundamental model, is the local equilibrium distribution function f_e :

$$f_e = \frac{n}{(\pi T)^{3/2}} \exp\left(-\frac{(\mathbf{c} - \mathbf{u})^2}{T}\right) \quad (2)$$

where n is the number density, \mathbf{u} the macroscopic flow velocity, and T the temperature. For a higher order model equation which correctly resembles the lower 13 moments of the Boltzmann equation [14], the distribution function f_0 is given as

$$f_0 = f_e \left[1 + 2(1 - Pr) \frac{(\mathbf{c} - \mathbf{u}) \cdot \mathbf{q}}{5pT} \left(\frac{2(\mathbf{c} - \mathbf{u})^2}{T} - 5 \right) \right] \quad (3)$$

where p is the pressure, \mathbf{q} the heat flux vector, and Pr the Prandtl number ($=2/3$ for a monatomic gas).

The macroscopic flow quantities are obtained from the distribution function as

$$\begin{aligned} n &= \int f d\mathbf{c} \\ n\mathbf{u} &= \int \mathbf{c} f d\mathbf{c} \\ \frac{3}{2}nT &= \int (\mathbf{c} - \mathbf{u})^2 f d\mathbf{c} \\ \mathbf{q} &= \int (\mathbf{c} - \mathbf{u})(\mathbf{c} - \mathbf{u})^2 f d\mathbf{c} \end{aligned} \quad (4)$$

The pressure p is obtained from the equation of state:

$$p = nT \quad (5)$$

All these quantities are normalized with a reference length L , a reference number density n_∞ , a reference temperature T_∞ , and a reference velocity C_∞ . The reference velocity C_∞ is the most probable molecular thermal speed which is defined as:

$$C_\infty = \sqrt{2RT_\infty} \quad (6)$$

The collision frequency ν is usually defined as:

$$\nu = \frac{8nT^{1-s}}{5\sqrt{\pi}Kn} \quad (7)$$

where Kn is the reference Knudsen number based on the reference length L and the molecular mean free path λ_∞ at reference state which is defined as

$$\lambda_\infty = \frac{16\mu_\infty}{5mn_\infty\sqrt{2\pi RT_\infty}} \quad (8)$$

where μ is the viscosity coefficient, m the mass of a molecule, and R the gas constant. The viscosity coefficient is assumed to depend on the temperature as:

$$\mu \propto T^s \quad (9)$$

where the Maxwell molecules correspond to the power s of 1 and the hard sphere molecules to 0.5. In this study, the hard sphere molecules is adopted.

For two dimensional flow problems, the following reduced distribution functions g and h are conveniently introduced so that the operational count and storage of the computation can be reduced.

$$g(t, x, y, c_x, c_y) = \int f dc_z \quad (10)$$

$$h(t, x, y, c_x, c_y) = \int c_z^2 f dc_z$$

The kinetic model Boltzmann equation (1) can be rewritten for the reduced distribution functions g and h as:

$$\frac{\partial g}{\partial t} + c_x \frac{\partial g}{\partial x} + c_y \frac{\partial g}{\partial y} = \nu(g_0 - g) \quad (11)$$

$$\frac{\partial h}{\partial t} + c_x \frac{\partial h}{\partial x} + c_y \frac{\partial h}{\partial y} = \nu(h_0 - h)$$

The distribution functions g_0 and h_0 can be obtained from equations (3) and (10) as:

$$g_0 = g_e \left[1 + 2(1 - Pr) \frac{(c_x - u)q_x + (c_y - v)q_y}{5pT} \left(\frac{2(\mathbf{c} - \mathbf{u})^2}{T} - 4 \right) \right] \quad (12)$$

$$h_0 = \frac{T}{2} g_e \left[1 + 2(1 - Pr) \frac{(c_x - u)q_x + (c_y - v)q_y}{5pT} \left(\frac{2(\mathbf{c} - \mathbf{u})^2}{T} - 2 \right) \right]$$

with the reduced local equilibrium distribution function g_e :

$$g_e = \frac{n}{\pi T} \exp \left(-\frac{(c_x - u)^2 + (c_y - v)^2}{T} \right) \quad (13)$$

The macroscopic flow quantities are obtained from the reduced distribution function as:

$$n = \int \int g dc_x dc_y$$

$$n(u, v)^T = \int \int (c_x, c_y)^T g dc_x dc_y \quad (14)$$

$$\frac{3}{2} nT = \int \int [(c_x - u)^2 + (c_y - v)^2] g dc_x dc_y$$

$$(q_x, q_y)^T = \int \int (c_x - u, c_y - v)^T [(c_x - u)^2 + (c_y - v)^2] g dc_x dc_y + \int \int h dc_x dc_y$$

2.2 Numerical procedure

Any conventional numerical methods, such as finite difference, finite volume, and finite element methods can be adopted for the solution of the kinetic model Boltzmann equation. In this study an upwind gridless method [16, 17] is adopted for estimation of the convective terms of the equation.

Gradients of any function f at a computational point i may be evaluated with the following linear combination form in the cloud of neighboring points $C(i)$.

$$\nabla f = \sum_{k \in C(i)} \mathbf{a}_{ik} f_{ik} \quad (15)$$

where the subscript k denotes the index of the point which belongs to the cloud $C(i)$. The sum is obtained over all member points of $C(i)$ except the point i itself. The function values f_{ik} are evaluated at the midpoint between the points i and k .

The coefficients \mathbf{a}_{ik} are once obtained at the beginning of computation and stored if the points remain stationary. Several methods can be used for obtaining the coefficients. If the approximation (15) is applied in a finite volume cell, the coefficients may be obtained from the unit normal and area of the cell surface, and the cell volume. If the approximation (15) is applied for points distributed arbitrarily, the x-component of the coefficients, for an example, a_{xik} can be obtained with solving the following system of equations using QR or singular value decompositions.

$$\sum_{k \in C(i)} a_{xik} f_{ik}^{(m)} = d^{(m)} \quad (16)$$

Here the components of $f^{(m)}$ and $d^{(m)}$ are given with:

$$f^{(m)} \in (1, x, y, z, x^2, y^2, z^2, xy, \dots) \quad (17)$$

and

$$d^{(m)} \in (0, 1, 0, 0, 0, 0, 0, 0, \dots) . \quad (18)$$

The convective terms of the kinetic model equations (11) can be evaluated with the gridless method, for an example, as:

$$\begin{aligned} \left(c_x \frac{\partial g}{\partial x} + c_y \frac{\partial g}{\partial y} \right) \Big|_i &= \sum_{k \in C(i)} (a_{xik} c_x + a_{yik} c_y) g_{ik} \\ &= \sum_{k \in C(i)} \xi_{ik} g_{ik} \end{aligned} \quad (19)$$

where ξ_{ik} is defined as:

$$\xi_{ik} = a_{xik} c_x + a_{yik} c_y \quad (20)$$

The numerical flux $\xi_{ik}g_{ik}$ are estimated as

$$\xi_{ik}g_{ik} = \frac{1}{2} \left\{ \xi_{ik}(g_{ik}^+ + g_{ik}^-) - |\xi_{ik}|(g_{ik}^+ - g_{ik}^-) \right\} \quad (21)$$

The third order accurate weighted essentially non-oscillatory (WENO) method [18] is used for reconstructing the midpoint distribution function g_{ik}^\pm [19].

After evaluating the convective and collision terms, following implicit Euler method is used for the temporal discretization of the kinetic model equation.

$$\left(\frac{1}{\Delta t_i} + \nu + \sum_{k \subset C(i)} \xi_{ik}^+ \right) \Delta g_i + \sum_{k \subset C(i)} \xi_{ik}^- \Delta g_k = RHS_i \quad (22)$$

where RHS are the evaluation of the convective and collision terms and ξ^\pm are defined as follows

$$\xi^\pm = \frac{1}{2}(\xi \pm |\xi|) \quad (23)$$

The solution of this linear system of equation (22) can be obtained with a lower-upper symmetric Gauss-Seidel (LU-SGS) procedure [20] as:

$$\Delta g_i^* = D_i^{-1} \left(RHS_i - \sum_{k \subset L(i)} \xi_{ik}^- \Delta g_k \right) \quad (24)$$

$$\Delta g_i = \Delta g_i^* - D_i^{-1} \sum_{k \subset U(i)} \xi_{ik}^- \Delta g_k \quad (25)$$

where $C(i) = L(i) \cup U(i)$ and D_i are defined with

$$D_i = \left(\frac{1}{\Delta t_i} + \nu + \frac{1}{2} \sum_{k \subset C(i)} |\xi_{ik}| \right) \quad (26)$$

The distribution function at the next time step g^{n+1} is obtained as:

$$g_i^{n+1} = g_i^n + \Delta g_i \quad (27)$$

where the superscript n denotes the time index.

The macroscopic flow quantities, for example, the number density, can be obtained with numerical quadrature as

$$n = \int \int g \, dc_x \, dc_y = \sum w g \quad (28)$$

where w are the weights of quadrature. Simple equally spaced trapezoidal rule is used in this study.

2.3 Boundary conditions

Perfect diffuse reflection is assumed for the interaction between molecules and solid walls. That is, molecules which strike the solid surface are subsequently emitted with fully accommodating to the wall temperature T_w and velocity (u_w, v_w) . The reduced distribution function g for the molecules reflecting from the wall surface is given by:

$$g_w = \frac{n_w}{\pi T_w} \exp\left(-\frac{(c_x - u_w)^2 + (c_y - v_w)^2}{T_w}\right) \quad c_n > 0 \quad (29)$$

The density of molecules diffusing from the surface is determined from the following mass balance condition:

$$\int \int_{c_n > 0} c_n g_w dc_x dc_y = - \int \int_{c_n < 0} c_n g dc_x dc_y \quad (30)$$

Substituting (29) into the left hand side of (30) and applying the numerical quadrature to both the integrals, the density can be obtained as:

$$n_w = -\frac{1}{\Theta} \sum_{c_n < 0} w c_n g \quad (31)$$

At the beginning of computation, Θ are once obtained from the following equation and stored at each point on the wall surface.

$$\Theta = \sum_{c_n > 0} \frac{w c_n}{\pi T_w} \exp\left(-\frac{(c_x - u_w)^2 + (c_y - v_w)^2}{T_w}\right) \quad (32)$$

At inlet and outlet boundaries, the local equilibrium distribution functions are specified for incoming molecules. For outgoing molecules, simple extrapolation of the distribution function is used, which may not affect numerical results because the distribution functions on inner computational points are updated with the upwind gridless solver.

3 CONTINUUM APPROACH

The basic equations of continuum approach is the compressible Navier-Stokes equations which may be written in the following nondimensional form.

$$\frac{\partial \mathbf{Q}}{\partial t} + \nabla \cdot \mathbf{F} = \frac{1}{Re} \nabla \cdot \mathbf{R} \quad (33)$$

where \mathbf{Q} is the conservative vector, \mathbf{F} the convective flux, \mathbf{R} the viscous flux, and Re the reference Reynolds number. The conservative vector and the flux terms are given with:

$$\mathbf{Q} = \begin{pmatrix} \rho \\ \mathbf{u} \\ e \end{pmatrix}, \quad \mathbf{F} = \begin{pmatrix} \rho \mathbf{u} \\ \rho \mathbf{u} \mathbf{u} + p \mathbf{I} \\ \mathbf{u}(e + p) \end{pmatrix}, \quad \mathbf{R} = \begin{pmatrix} 0 \\ \tau \\ \mathbf{u} \cdot \tau - \mathbf{q} \end{pmatrix} \quad (34)$$

where e is the total energy per unit volume, which is given for a perfect gas as:

$$e = \frac{p}{\gamma - 1} + \frac{1}{2}\rho\mathbf{u}^2 \quad (35)$$

Here γ is the ratio of specific heats. The viscous stress tensor τ and the heat flux vector \mathbf{q} are defined with:

$$\tau_{ij} = \mu \left(\frac{\partial u_i}{\partial x_j} + \frac{\partial u_j}{\partial x_i} - \frac{2}{3}\delta_{ij} \frac{\partial u_i}{\partial x_j} \right) \quad (36)$$

$$q_i = -\frac{\gamma}{\gamma - 1} \frac{\mu}{Pr} \frac{\partial T}{\partial x_i} \quad (37)$$

All these quantities in the continuum approach are normalized with a reference length L , a reference density ρ_∞ ($= mn_\infty$), a reference temperature T_∞ , and a reference velocity U_∞ . The reference velocity U_∞ is defined as:

$$U_\infty = \sqrt{RT_\infty} \quad (38)$$

where nondimensional velocities in the continuum approach are greater than those in the kinetic approach by the ratio of $\sqrt{2}$.

The Navier-Stokes equations are also solved using the upwind gridless and LU-SGS methods [16, 17]. The convective terms are evaluated with:

$$\begin{aligned} \nabla \cdot \mathbf{F}|_i &= \sum_{k \subset \mathcal{C}(i)} (\mathbf{a}_{ik} \cdot \mathbf{F}_{ik}) \\ &= \sum_{k \subset \mathcal{C}(i)} \mathbf{G}_{ik} \end{aligned} \quad (39)$$

The flux term \mathbf{G} at the midpoint between the point i and point j is expressed for two dimensional flows as:

$$\mathbf{G} = \begin{pmatrix} \rho U \\ \rho u U + a_x p \\ \rho v U + a_y p \\ U(e + p) \end{pmatrix} \quad (40)$$

where U is defined by

$$U = a_x u + a_y v \quad (41)$$

The numerical flux G_{ik} are estimated as:

$$\mathbf{G}_{ik} = \frac{1}{2} \left\{ \mathbf{G}(\tilde{\mathbf{Q}}_{ik}^+) + \mathbf{G}(\tilde{\mathbf{Q}}_{ik}^-) - |\tilde{\mathbf{A}}_{ik}| (\tilde{\mathbf{Q}}_{ik}^+ - \tilde{\mathbf{Q}}_{ik}^-) \right\} \quad (42)$$

where \tilde{Q} are the primitive variables defined as:

$$\tilde{\mathbf{Q}} = \begin{pmatrix} \rho \\ u \\ v \\ p \end{pmatrix} \quad (43)$$

The flux Jacobian matrices $\tilde{\mathbf{A}}$ is introduced as:

$$\tilde{\mathbf{A}} = \frac{\partial \mathbf{G}}{\partial \tilde{\mathbf{Q}}} \quad (44)$$

and

$$|\tilde{\mathbf{A}}| = \tilde{\mathbf{X}} |\tilde{\mathbf{\Lambda}}| \tilde{\mathbf{X}}^{-1} \quad (45)$$

Here $\tilde{\mathbf{\Lambda}}$ are the eigenvalue matrices and $\tilde{\mathbf{X}}^{-1}$ are the right eigenvector matrices. The primitive variables $\tilde{\mathbf{Q}}_{ik}^\pm$ at the midpoint are reconstructed with the third order accurate WENO method [19].

The viscous terms of the Navier-Stokes equations are also evaluated with the gridless method, for an example, as:

$$\left. \frac{\partial}{\partial x} \left(\mu \frac{\partial u}{\partial x} \right) \right|_i = \sum_{k \in C(i)} a_{xik} \left(\mu \frac{\partial u}{\partial x} \right)_{ik} \quad (46)$$

While a simple arithmetical average is used for obtaining μ_{ik} , the first derivatives at the midpoint is evaluated with the following method.

$$\left. \frac{\partial u}{\partial x} \right|_{ik} = \frac{\Delta x}{\Delta s^2} (u_k - u_i) + \frac{1}{2} \frac{\Delta y}{\Delta s^2} \left[\Delta y \left(\left. \frac{\partial u}{\partial x} \right|_i + \left. \frac{\partial u}{\partial x} \right|_k \right) - \Delta x \left(\left. \frac{\partial u}{\partial y} \right|_i + \left. \frac{\partial u}{\partial y} \right|_k \right) \right] \quad (47)$$

where Δx , Δy , and Δs^2 are defined with:

$$\Delta x = x_k - x_i$$

$$\Delta y = y_k - y_i \quad (48)$$

$$\Delta s^2 = \Delta x^2 + \Delta y^2$$

After evaluating the convective and viscous terms, a linearized implicit Euler method is obtained for the temporal discretization of the Navier-Stokes equations as:

$$\left(\frac{1}{\Delta t_i} \mathbf{I} + \sum_{k \in C(i)} \mathbf{A}_{ik}^+(\mathbf{Q}_i^n) \right) \Delta \mathbf{Q}_i + \sum_{k \in C(i)} \mathbf{A}_{ik}^+(\mathbf{Q}_k^n) = \mathbf{RHS}_i \quad (49)$$

where **RHS** are the evaluation of the convective and viscous terms and the split flux Jacobian matrices \mathbf{A}^\pm are given with:

$$\mathbf{A}^\pm = \mathbf{X}\mathbf{\Lambda}^\pm\mathbf{X}^{-1} \quad (50)$$

The solution of this linear system of equation (49) is obtained with a LU-SGS procedure as:

$$\Delta\mathbf{Q}_i^* = \mathbf{D}_i^{-1} \left(\mathbf{RHS}_i - \sum_{k \subset L(i)} \mathbf{A}_{ik}^-(\mathbf{Q}_k^n) \Delta\mathbf{Q}_k^* \right) \quad (51)$$

$$\Delta\mathbf{Q}_i = \Delta\mathbf{Q}_i^* - \mathbf{D}_i^{-1} \sum_{k \subset U(i)} \mathbf{A}_{ik}^-(\mathbf{Q}_k^n) \Delta\mathbf{Q}_k \quad (52)$$

where D_i are defined with

$$\mathbf{D}_i = \left(\frac{1}{\Delta t_i} \mathbf{I} + \sum_{k \subset C(i)} \mathbf{A}_{ik}^+(\mathbf{Q}_i^n) \right) \quad (53)$$

At the wall surface, the first order slip conditions are implemented as:

$$u_s - u_w = \frac{2 - \sigma_v}{\sigma_v} Kn \frac{\mu}{\rho \sqrt{T_w}} \frac{\partial u}{\partial n} + \frac{3}{4} \sqrt{\frac{\pi}{2}} Kn \frac{\mu}{\rho T_w} \frac{\partial T}{\partial s} \quad (54)$$

$$T_s - T_w = \frac{2 - \sigma_t}{\sigma_t} \frac{2\gamma}{\gamma + 1} \frac{Kn}{Pr} \frac{\mu}{\rho \sqrt{T_w}} \frac{\partial T}{\partial n} \quad (55)$$

where n and s denote the normal and tangential directions to the surface, respectively. The momentum accommodation coefficient σ_v and the energy accommodation coefficient σ_t are set to unity in all the computation presented here.

For inlet and outlet boundaries, characteristic boundary conditions are implemented.

4 CONTINUUM/KINETIC HYBRID APPROACH

Domain decomposition strategy is adopted for the continuum/kinetic hybrid approach. A multi-scale computational domain is decomposed into the continuum regions and the kinetic regions. Since computational points (cells) belong to either the continuum regions or the kinetic regions, no overlapping points exist in this study. The Navier-Stokes solver works on the points in the continuum regions and the kinetic model Boltzmann solver in the kinetic regions.

At the interface between the continuum and kinetic regions, information exchange is necessary at every time step over the two layers of either side of the interface, because the stencil of the third order accurate WENO reconstruction is generally five. At the points in the continuum regions two layer inside from the interface, the following Chapman-Enskog distribution functions for the kinetic model Boltzmann equations (1) with (3) are constructed.

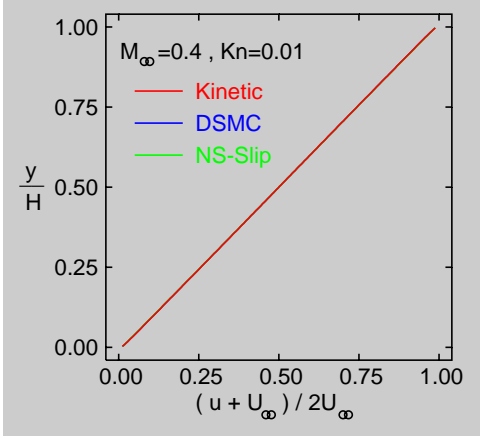


Figure 1: Comparison of velocity profiles for a Couette flow at $M_\infty = 0.4$ and $Kn = 0.01$.

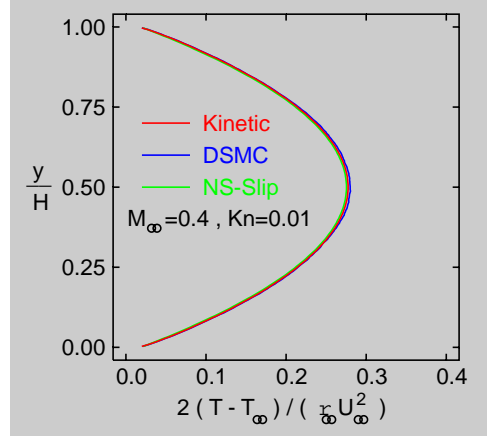


Figure 2: Comparison of temperature profiles for a Couette flow at $M_\infty = 0.4$ and $Kn = 0.01$.

$$f = f_e \left\{ 1 - \frac{1}{\nu} \left[\frac{\tau_{ij} (c_i - u_i)(c_j - v_j)}{\mu T} + \frac{1}{Pr} \left(\frac{(\mathbf{c} - \mathbf{u})^2}{T} - \frac{5}{2} \right) \frac{c_i - u_i}{T} \frac{\partial T}{\partial x_i} \right] \right\} \quad (56)$$

On the other hand, the numerical flux of the Navier-Stokes equations can be simply evaluated over the interface, since the macroscopic flow quantities are obtained using the equation (14) at every time step even in the kinetic regions. For conservation of numerical flux, however, the numerical flux \mathbf{G}_{ik} of the equation (39) at the interface is replaced with the following flux obtained from the corresponding flux of the kinetic model Boltzmann equations.

$$\mathbf{G}_{ik} = \begin{pmatrix} \sqrt{2} \iint \xi_{ik} g_{ik} \, dc_x \, dc_y \\ 2 \iint c_x \xi_{ik} g_{ik} \, dc_x \, dc_y \\ 2 \iint c_y \xi_{ik} g_{ik} \, dc_x \, dc_y \\ \sqrt{2} \iint [(c_x^2 + c_y^2) \xi_{ik} g_{ik} + \xi_{ik} h_{ik}] \, dc_x \, dc_y \end{pmatrix} \quad (57)$$

5 VARIDATION OF BOLTZMANN SOLVER

In order to validate the kinetic model Boltzmann solver as well as the Naiver-Stokes solver with the slip boundary conditions, Couette flows and supersonic flows over a circular cylinder are simulated and results are compared with those obtained with the DSMC method.

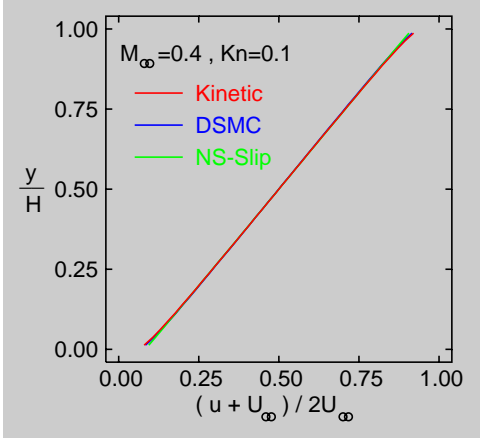


Figure 3: Comparison of velocity profiles for a Couette flow at $M_\infty = 0.4$ and $Kn = 0.1$.

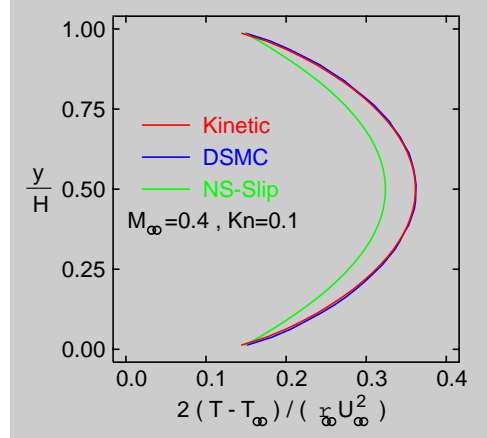


Figure 4: Comparison of temperature profiles for a Couette flow at $M_\infty = 0.4$ and $Kn = 0.1$.

5.1 Couette flow

Couette flow is a well defined benchmark problem to validate a numerical method. In this study, upper and lower parallel plates move in the opposite direction each other with the velocity U_∞ and $-U_\infty$, respectively. The reference length is the distance between the two plates. Figures 1 and 2 show the comparison of the velocity and temperature profiles obtained at a Knudsen number of 0.01 and a Mach number, based on the plate speed, of 0.4. For this low Knudsen number case, the Navier-Stokes solver with the slip boundary conditions predicts good results compared to those predicted with the Boltzmann solver and the DSMC method.

Similar comparison is made at a Knudsen number of 0.1 in Figs. 3 and 4. The Mach number based on the plate speed is unchanged at 0.4. While the Navier-Stokes solver predicts the velocity profile well except for the slight difference observed just by the plates, it fails to predict the temperature profile at this moderate Knudsen number case. Comparison between the results of the Boltzmann solver and those of the DSMC method is still quite good.

5.2 Supersonic flow over a circular cylinder

Supersonic flows about a circular cylinder at a free stream Mach number of 2.0 and Knudsen numbers of 0.01 and 0.1 are simulated. The Knudsen number is estimated based on the diameter of the circular cylinder and the reference mean free path at the free stream. The results obtained with the kinetic model Boltzmann solver, the slip Navier-Stokes solver, and the DSMC method are compared with one another.

Figures 5 and 6 show the comparison of the density contours and temperature contours, respectively. The results are obtained at the free stream Knudsen number of 0.01. While the computations are carried out for the whole two dimensional domain with 1024×512

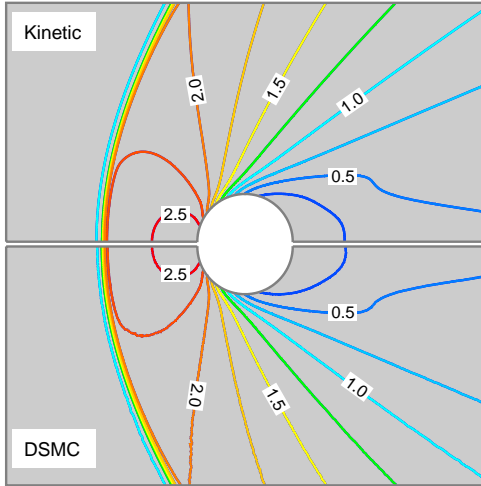


Figure 5: Density contours obtained with kinetic model Boltzmann solver and DSMC method at $M_\infty = 2.0$ and $Kn = 0.01$.

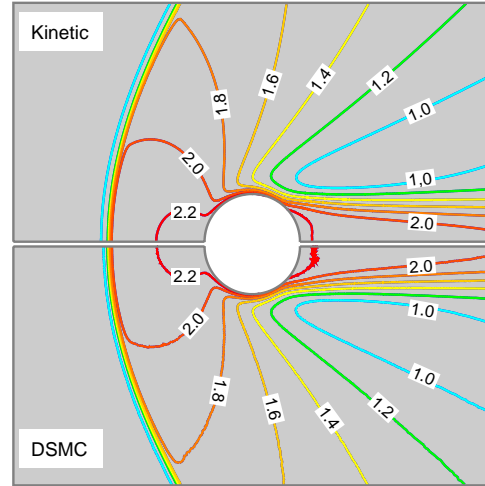


Figure 6: Temperature contours obtained with kinetic model Boltzmann solver and DSMC method at $M_\infty = 2.0$ and $Kn = 0.01$.

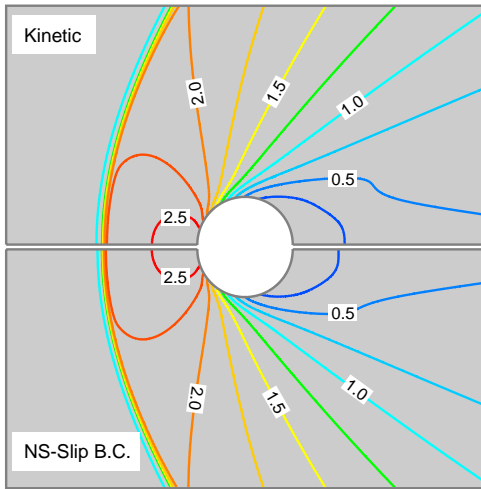


Figure 7: Density contours obtained with kinetic model Boltzmann solver and slip NS solver at $M_\infty = 2.0$ and $Kn = 0.01$.

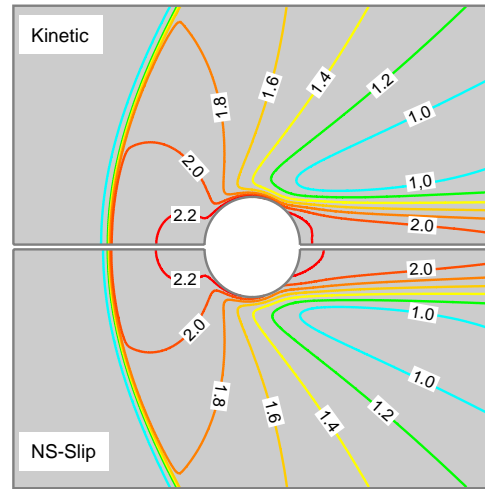


Figure 8: Temperature contours obtained with kinetic model Boltzmann solver and slip NS solver at $M_\infty = 2.0$ and $Kn = 0.01$.

cells, the results of the kinetic model Boltzmann solver are plotted for the upper half domain and the DSMC results for the lower half domain. Very good agreement between the kinetic model results and the DSMC results is generally observed over the whole flow field.

Comparison between the kinetic model results and the slip Navier-Stokes results is made in Figs. 7 and 8. At this low Knudsen number, the comparison between the kinetic results and the continuum results is quite good in the whole flow field except for the slight

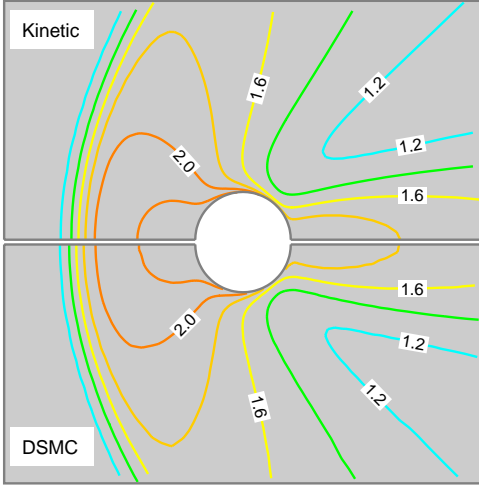


Figure 9: Temperature contours obtained with kinetic model Boltzmann solver and DSMC method at $M_\infty = 2.0$ and $Kn = 0.1$.

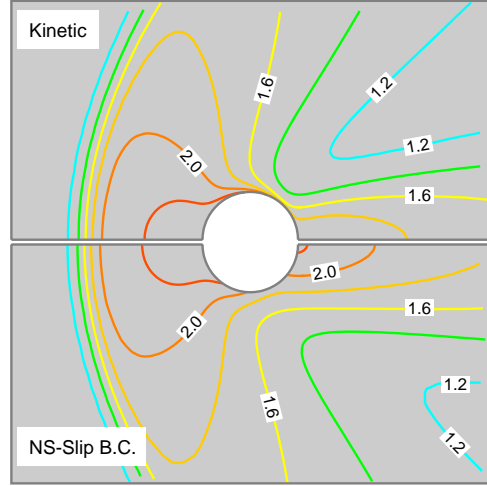


Figure 10: Temperature contours obtained with kinetic model Boltzmann solver and slip NS solver at $M_\infty = 2.0$ and $Kn = 0.1$.

difference observed just behind the circular cylinder, where the density is lower than the free stream density and the rarefactive effect may be pronounced.

Temperature contours obtained at a free stream Mach number of 2.0 and a Knudsen number of 0.1 are compared in Figs. 9 and 10. Each computation is carried out for the whole two dimensional domain with 128×64 cells. Figure 9 shows the comparison between the kinetic results and the DSMC results. The comparison is still quite good over the whole flow field. Figure 10 shows the comparison between the kinetic results and the continuum results. Although the continuum results fail to predict the temperature distribution in the wake region, the results in front region are fairly good.

Figure 11 shows the comparison of temperature contours obtained with the kinetic model Boltzmann solver and the DSMC method at a higher free stream Knudsen number of 1.0. If the Knudsen number is not small, there may be no theoretical guarantee for the kinetic model collision operator. The comparison between the kinetic model results and the DSMC results, however, is generally good even for the high Knudsen number flow case.

Figure 12 shows the drag coefficients as a function of the Knudsen number. In addition to the three numerical results, the experiments of Maslach and Schaaf [21] are plotted with square symbols. Very good agreement between the kinetic model results and the DSMC results is again observed. The results of the Navier-Stokes equations with slip boundary conditions well agree with the kinetic model results if the Knudsen number is less than 0.1.

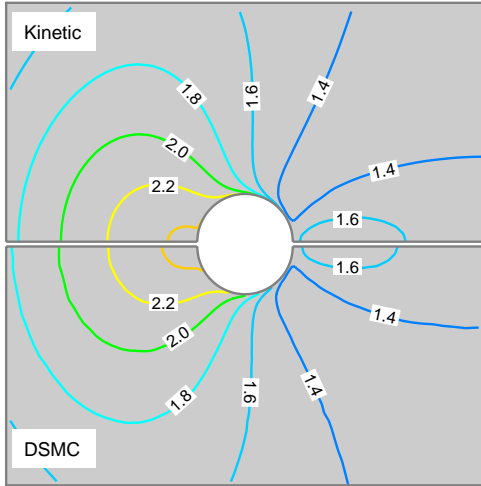


Figure 11: Temperature contours obtained with kinetic model Boltzmann solver and DSMC method at $M_\infty = 2.0$ and $Kn = 1.0$.

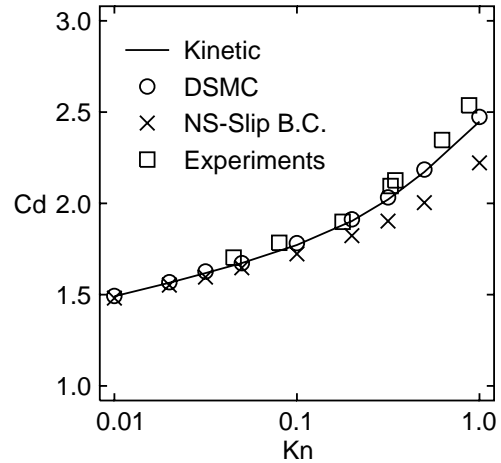


Figure 12: Comparison of drag coefficients as a function of Knudsen number.

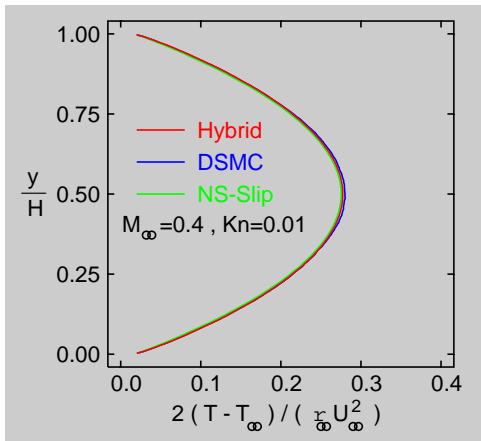


Figure 13: Comparison of temperature profiles for a Couette flow at $M_\infty = 0.4$ and $Kn = 0.01$.

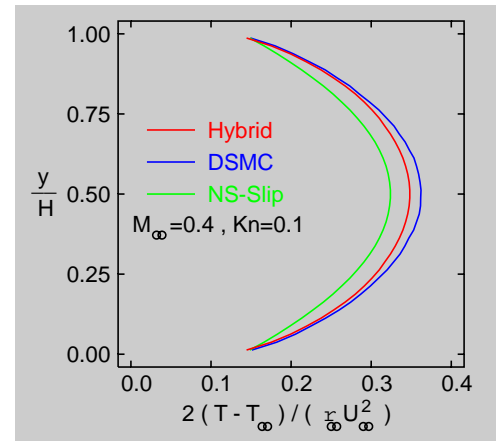


Figure 14: Comparison of temperature profiles for a Couette flow at $M_\infty = 0.4$ and $Kn = 0.1$.

6 VARIDATION OF CONTINUUM/KINETIC HYBRID SOLVER

Validation of the continuum/kinetic hybrid solver are carried out for the Couette flows and the supersonic flow over a circular cylinder. The results are compared with those obtained with the full kinetic solver, the full Navier-Stokes solver, and the DSMC method.

6.1 Couette flow

Figure 13 shows the comparison of the temperature profiles obtained at the Knudsen number of 0.01 and the plate speed Mach number of 0.4. The continuum/kinetic interface

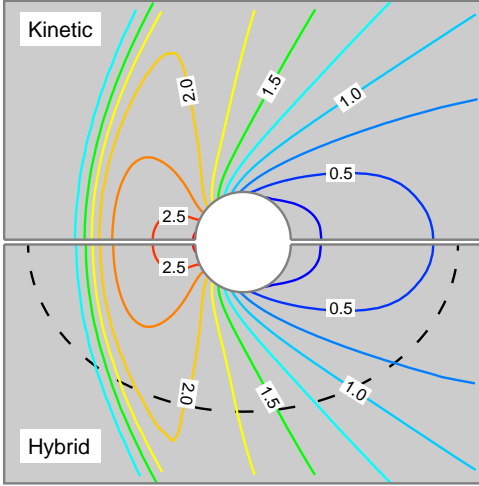


Figure 15: Density contours obtained with full kinetic solver and continuum/kinetic hybrid solver at $M_\infty = 2.0$ and $Kn = 0.1$.

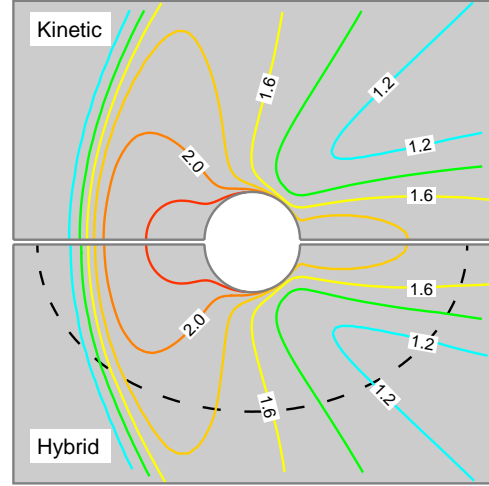


Figure 16: Temperature contours obtained with full kinetic solver and continuum/kinetic hybrid solver at $M_\infty = 2.0$ and $Kn = 0.1$.

in the hybrid solver is located at 10 mean free path away from each plate. Since neither oscillation nor wiggle are found in the temperature distribution, it is confirmed that the continuum/kinetic coupling works quite well.

Figure 14 shows the comparison of the temperature distribution obtained at the higher Knudsen number of 0.1 and the Mach number based on the plate speed of 0.4. Since the distance between the two plates is 10 mean free path at this Knudsen number, the interface between the continuum and kinetic regions in the hybrid solver is located at only 2.5 mean free path away from each plate. Although the results of the continuum/kinetic hybrid solver seem to be better than the results of the full continuum solver, the full kinetic solver is preferable for the Couette flow at this Knudsen number.

6.2 Supersonic flow over a circular cylinder

The continuum/kinetic hybrid simulation is carried out for the supersonic flow about a circular cylinder at a free stream Mach number of 2.0 and a Knudsen number of 0.1. The results are compared with those obtained with the full kinetic model Boltzmann solver. Figures 15 and 16 show the comparison of the density contours and temperature contours, respectively. In the hybrid method, the solution is computed with the kinetic model Boltzmann equation on the inner field of broken line circle and with the Navier-Stokes equations on the outer field. Although, as is seen in Fig. 10, the full continuum results fail to predict the temperature distribution in the wake region at this Knudsen number, the continuum/kinetic hybrid solver succeeds in predicting the density and temperature contours over the whole flow field.

7 CONCLUSIONS

A continuum/kinetic hybrid approach is developed for simulating the continuum to free molecule, multi-scale flows. Domain decomposition strategy is adopted for coupling the continuum and kinetic approaches. A multi-scale computational domain is decomposed into the continuum regions and the kinetic regions. A compressible Navier-Stokes solver is adopted for the continuum regions, while a deterministic solver based on a kinetic model Boltzmann equation is adopted for the kinetic regions. The continuum/kinetic coupling works quite well. The hybrid solver produces reliable solution for both subsonic and supersonic flows at lower computational costs compared to the direct simulation Monte Carlo method. Numerical results obtained with the hybrid solver have been compared with those of the Navie-Stokes solver for slip flow regime and those of the direct simulation Monte Carlo method for rarefied flow regime. The comparison is fairly good.

This study was partly supported by a Grant-in-Aid for Scientific Research (17360079) from the Japan Society for the Promotion of Science.

REFERENCES

- [1] D.B. Hash and H.A. Hassan. Assessment of schemes for coupling Monte Carlo and Navier-Stokes solution methods. *Journal of Thermophysics and Heat Transfer*, **10**, 242–249, (1996).
- [2] P.L. Tallec and F. Mallinger. Coupling Boltzmann and Navier-Stokes equations by half fluxes. *Journal of Computational Physics*, **136**, 51–67, (1997).
- [3] S. Tiwari. Coupling of the Boltzmann and Euler equations with automatic domain decomposition. *Journal of Computational Physics*, **144**, 710–726, (1998).
- [4] A.L. Garcia, J.B. Bell, W.Y. Crutchfield, and B.J. Alder. Adaptive mesh and algorithm refinement using direct simulation Monte Carlo. *Journal of Computational Physics*, **154**, 134–155, (1999).
- [5] O. Aktas and N.R. Aluru. A combined continuum/DSMC technique for multiscale analysis of microfluidic filters. *Journal of Computational Physics*, **178**, 342–372, (2002).
- [6] Q. Sun, I.D. Boyd, and G.V. Candler. A hybrid continuum/particle approach for modeling subsonic, rarefied gas flows. *Journal of Computational Physics*, **194**, 256–277, (2004).
- [7] T.E. Schwartzentruber and I.D. Boyd, A hybrid particle-continuum method applied to shock waves. *Journal of Computational Physics*, **215**, 402–416, (2006).

- [8] G.A. Bird. *Molecular gas dynamics and the direct simulation of gas flows*, Oxford Science Publications, (1994).
- [9] E.S. Oran, C.K. Oh, and B.Z. Cybyk. Direct simulation monte carlo: Recent advances and applications. *Annual Review of Fluid Mechanics*, **30**, 403–442, (1998).
- [10] J. Fan, I.D. Boyd, C.P. Cai. Computation of rarefied gas flows around a NACA0012 airfoil. *AIAA Journal*, **39**, 618–625, (2001).
- [11] K. Morinishi and H. Oguchi. A Computational method and its application to analyses of rarefied gas flows. *Proc. 14th International Symposium on Rarefied Gas Dynamics*, University of Tokyo Press, Vol. 1, 149–158, (1984).
- [12] K. Morinishi. Numerical simulation for gas microflows using Boltzmann equation. *Computers & Fluids*, **35**, 978–985, (2006).
- [13] N. Satofuka, K. Morinishi, and T. Oishi. Numerical solution of the kinetic model equations for hypersonic flows. *Computational Mechanics*, **11**, 452–464, (1993).
- [14] T. Abe and H. Oguchi. A hierarchy kinetic model and its applications. *Proc. 10th International Symposium on Rarefied Gas Dynamics*, Progress in Astronautics and Aeronautics, AIAA, **58** 781–793, (1977).
- [15] P.L. Bhatnager, E.P. Gross, and M. Krook. A model collision processes in gases. I. Small amplitude processes in charged and neutral one-component system, *Physical Review*, **94**, 511–525, (1954).
- [16] K. Morinishi. A Gridless type solver - Generalized finite difference method -. *Computational Fluid Dynamics for the 21st Century*, Notes on Numerical Fluid Mechanics, Springer, **78**, 43–58, (2001).
- [17] K. Morinishi. Parallel computation of gridless type solver for unsteady flow problems. *Parallel Computational Fluid Dynamics*, Elsevier, 275–284, (2002).
- [18] G.S. Jiang and C.W. Shu. Efficient implementation of weighted ENO schemes. *Journal of Computational Physics*, **126**, 202–228, (1996).
- [19] K. Morinishi. Parallel computation of higher order gridless type solver. *Parallel Computational Fluid Dynamics*, Elsevier, 427–434, (2003).
- [20] A. Jameson and S. Yoon. Lower-upper implicit schemes with multiple grids for the Euler equations, *AIAA Journal*, **25**, 929–935, (1987).
- [21] G.J. Maslach and S.A. Schaaf. Cylinder drag in the transition from continuum to free-molecule flow, *Physics of Fluids*, **6**, 315–321, (1963).